

Performance Analysis of Multi-User Massive MIMO Downlink under Channel Non-Reciprocity and Imperfect CSI

Orod Raeesi, *Student Member, IEEE*, Ahmet Gokceoglu, *Member, IEEE*,
Yaning Zou, *Member, IEEE*, and Mikko Valkama, *Senior Member, IEEE*

Abstract

This paper analyzes the performance of linearly precoded time division duplex based multi-user massive MIMO downlink system under joint impacts of channel non-reciprocity (NRC) and imperfect channel state information (CSI). We consider a practical NRC model which accounts for transceiver frequency-response mismatches at both user equipment (UE) and base station (BS) sides as well as mutual coupling mismatches at BS. The analysis covers two most prominent forms of linear precoding schemes, namely, zero-forcing (ZF) and maximum-ratio transmission (MRT), and assumes that the statistical channel properties are used in the user side to decode the received signal. Closed-form analytical expressions are derived for the effective signal to interference and noise ratios (SINRs) and the corresponding capacity lower bounds, stemming from the developed signal and system models. The

O. Raeesi, A. Gokceoglu, and M. Valkama are with the Department of Electronics and Communications Engineering, Tampere University of Technology, Tampere 33720, Finland (e-mail: orod.raeesi@tut.fi; ahmet.gokceoglu@tut.fi; mikko.e.valkama@tut.fi).

Y. Zou is with Technische Universität Dresden, Vodafone Chair Mobile Communications Systems, Dresden, Germany (e-mail: yaning.zou@ifn.et.tu-dresden.de).

This work was supported by the Finnish Funding Agency for Technology and Innovation (Tekes) under the project “5th Evolution Take of Wireless Communication Networks (TAKE-5)” and by the Academy of Finland under the projects 284694 and 288670.

This work has been submitted to IEEE for possible publication. Copyright may be transferred without notice, after which this version may no longer be accessible.

derived analytical expressions show that, in moderate to high SNR region, the additional interference caused by practical NRC levels degrades the performance of both precoders significantly. Moreover, the ZF is shown to be more sensitive to NRC with a much more severe performance loss compared to MRT. Numerical evaluations with practical NRC levels indicate that this performance loss in the received SINR can be as high as 80% for ZF, whereas it is typically less than 20% for MRT. The derived analytical expressions provide useful tools, e.g., in calculating the NRC calibration requirements in BSs and UEs for given specific performance targets in terms of the system capacity lower bound or effective SINR.

Index Terms

Capacity, channel reciprocity, frequency-response mismatch, linear precoding, multi-user massive MIMO, mutual coupling, SINR.

I. INTRODUCTION

Massive multiple-input multiple-output (MIMO) systems are envisioned to be one key enabling technology for the next generation cellular networks known as 5G [1], [2]. In massive MIMO systems, a base station (BS) uses a large antenna array with dimension N to serve K user equipments (UEs) simultaneously on the same time-frequency resource, where typically $N \gg K$ [2]–[5]. Large-scale system analysis shows that linear precoding techniques, e.g., zero-forcing (ZF) and maximum ratio transmission (MRT) are asymptotically optimal with increasing N , while very high spectral-efficiencies can already be achieved with N being in the order of several tens or hundreds [5]–[8].

The key requirement for employing the above precoding schemes is to have accurate channel state information (CSI) at BS. In conventional frequency-division duplex (FDD) based MIMO systems, where the number of antennas in BS is relatively low, UEs commonly estimate downlink (DL) channels based on the received DL training signals transmitted by BS, and send the estimated DL channel information back to the BS [9]. The number of DL pilots required for estimating the channel is proportional to the number of adopted antennas in the BS which complicates the adoption of such DL channel estimation and reporting methods in massive MIMO systems. As an alternative approach, massive MIMO systems

are typically assumed to employ time-division duplex (TDD), and thus estimate the DL channel based on uplink (UL) pilots, relying on the reciprocity of the physical DL and UL channels within each coherence interval [10]. Thereby, the required amount of resources in such TDD based approach is only proportional to the number of served UEs which is typically much smaller than the number of BS antennas, i.e., $K \ll N$ [5], [10].

The channel reciprocity in TDD systems holds strictly speaking only for the physical propagation channels. However, when the effective baseband-to-baseband transmission channels between the BS and UEs are considered, incorporating also the impacts of the involved transceiver circuits, the reciprocity does not hold anymore due to the mismatches in transmit and receive mode characteristics of the transceivers [11]–[14]. More specifically, such mismatch characteristics include the unavoidable differences between the frequency-responses (FRs) of transmitter and receiver chains of any individual transceiver, as well as mutual coupling effects between the antenna elements in multi-antenna devices [15]–[17]. The impacts of such transceiver hardware induced non-reciprocity, also commonly referred to as channel non-reciprocity (NRC), have been studied for massive MIMO systems to a certain extent in [18]–[22]. To this end, [18]–[21] study the system performance degradation in terms of signal to interference and noise ratios (SINRs) and the corresponding achievable rates due to NRC, while assuming otherwise ideal system with perfect CSI. Then, [22] studies the system performance under joint impacts of NRC and imperfect CSI. However, the system model in [22] considers only FR mismatch but does not address the NRC induced by possible mutual coupling mismatches, reported, e.g., in [15]–[17], [19] to be one practical source of non-reciprocity. Furthermore, only the BS side NRC is considered in [19], [20].

In this paper, we analyze the SINR and achievable rate performance of linearly precoded TDD multi-user massive MIMO DL transmission systems under joint impacts of imperfect CSI and NRC. We consider a generic and realistic NRC model which takes into account the FR mismatches at both the UEs and the BS together with mutual coupling mismatches at the BS. The analysis is carried out for the two most prominent forms of linear precoding, namely, ZF and MRT. As in [7], [22]–[24], we also

assume that UEs rely on statistical channel properties to decode the received signals. Based on the developed signal and system models, closed-form expressions are derived for the effective SINRs and the corresponding capacity lower bounds. To highlight the substantial differences between this work and the existing literature on performance analysis of NRC impaired massive MIMO systems, we summarize the novel contributions of this manuscript as follows:

- 1) In contrast to [18]–[21] which consider NRC alone, in this work we consider the joint impacts of NRC and imperfect CSI.
- 2) In contrast to the simplified NRC model in [22] which considers only FR mismatches, a more practical and generic NRC model is considered in this work which incorporates both FR and mutual coupling mismatches.
- 3) In contrast to [18]–[22], the derived analytical expressions decompose the total received interference into two parts, namely, interference power due to imperfect CSI, without NRC, and an additional interference term due to NRC (see expression (22) for ZF, and (27) for MRT). With this decomposition, it is straightforward to quantify the specific performance degradation due to NRC with respect to the ideal reciprocal case.
- 4) In contrast to [19], [21], a performance comparison between ZF and MRT precoding schemes is also carried out which shows the relative sensitivity of these precoders to different NRC levels.

Given specific performance targets, such as effective SINRs and/or capacity lower bound, the derived analytical expressions reported in this manuscript can be directly used in designing and dimensioning the system, e.g., choosing the appropriate precoder based on performance-complexity trade-off, deciding the number of active antenna elements, and/or extracting the needed accuracy of NRC calibration schemes.

The rest of the paper is organized as follows. Section II describes the fundamental multi-user massive MIMO system model with transceiver non-reciprocity and imperfect CSI. Then, in Section III, analytical expressions are derived for the effective DL SINR and capacity lower bound under ZF and MRT precoding schemes. In Section IV, the asymptotic SINR and achievable rate expressions are derived for ZF and MRT precoding schemes, and also an analytic performance comparison is pursued. In Section V,

extensive numerical evaluations are provided to verify the derived analytical expressions and illustrate the impact of various non-reciprocity parameters on the system performance. Finally, conclusions are drawn in Section VI. Selected details regarding the derivations of the reported analytic expressions are reported in an Appendix.

Notations: Throughout this paper, matrices (vectors) are denoted with upper (lower) bold characters, e.g., \mathbf{V} (\mathbf{v}). The superscripts $(\cdot)^T$, $(\cdot)^*$, and $(\cdot)^H$ stand for transpose, conjugate, and conjugate-transpose, respectively. Expectation operator is shown by $\mathbb{E}[\cdot]$, while $\text{Tr}(\cdot)$ represents the trace operator and $\text{Var}(\cdot)$ refers to the variance. \mathbf{I}_n and $\mathbf{0}_n$ denote $n \times n$ identity and all-zero matrices, respectively. The element in i -th row and j -th column of matrix \mathbf{V} is represented by v_{ij} . A diagonal matrix with elements (v_1, \dots, v_n) is shown by $\text{diag}(v_1, \dots, v_n)$, and finally $\mathcal{CN}(0, \sigma^2)$ represents a circularly symmetric zero-mean complex Gaussian distribution with variance σ^2 .

II. SYSTEM MODEL

We consider precoded downlink transmission in a TDD based multi-user massive MIMO system, where a BS with N antennas serves K single-antenna UEs simultaneously on the same time-frequency resource with $N \gg K$. We further assume that the spatial transmit signal vector is generated using linear precoding techniques, e.g., ZF or MRT. All signal and system models are written for an arbitrary subcarrier of the underlying orthogonal frequency division multiplexing/multiple access (OFDM/OFDMA) waveform, that is, before IFFT and after FFT on the TX and RX sides, respectively. It is further assumed that the cyclic prefix (CP) length is larger than the channel delay spread. For notational simplicity, the subcarrier index is not shown explicitly and thus an arbitrary subcarrier is considered.

A. Uplink Training, Downlink Transmission and Effective Channels

The linear precoder is designed based on the DL CSI acquired from UL pilots. The fundamental signal models for the UL pilot and DL data transmission phases can be expressed as

$$\text{UL} : \mathbf{Y}^p = \sqrt{\rho_u} \mathbf{G} \mathbf{X}^p + \mathbf{N}^p \quad (1)$$

$$\text{DL} : \mathbf{r} = \sqrt{\rho_d} \mathbf{H} \mathbf{x} + \mathbf{n},$$

where $\mathbf{G} \in \mathbb{C}^{N \times K}$ and $\mathbf{H} \in \mathbb{C}^{K \times N}$ are the effective UL and DL channel matrices, respectively. Regarding the UL signal model, ρ_u is the transmitted signal to noise ratio (SNR) of the UL pilots, $\mathbf{Y}^p = [\mathbf{y}_1^p, \dots, \mathbf{y}_N^p]^T$ is the received signal matrix at the BS receiver, stacking the received UL pilots over τ_u symbol durations, where $\mathbf{y}_n^p \in \mathbb{C}^{\tau_u \times 1}$ contains the received UL pilots at n -th BS antenna, and $\mathbf{N}^p = [\mathbf{n}_1^p, \dots, \mathbf{n}_N^p]^T$ is the additive receiver noise matrix at the BS with i.i.d $\mathcal{CN}(0, 1)$ elements, where $\mathbf{n}_n^p \in \mathbb{C}^{\tau_u \times 1}$ is the additive receiver noise at n -th BS antenna. The matrix stacking all the transmitted UL pilots from all the considered UEs is shown by $\mathbf{X}^p = [\mathbf{x}_1^p, \dots, \mathbf{x}_K^p]^T$, where $\mathbf{x}_k^p \in \mathbb{C}^{\tau_u \times 1}$ is the UL temporal pilot vector transmitted from k -th UE. Then, for the DL, $\mathbf{r} \in \mathbb{C}^{K \times 1}$ denotes the received DL signal vector corresponding to all K UEs, ρ_d is the transmitted SNR of DL channel, and $\mathbf{n} \in \mathbb{C}^{K \times 1}$ is the additive receiver noise vector at UE side with i.i.d $\mathcal{CN}(0, 1)$ elements. The precoded spatial transmit signal vector in the BS is shown by $\mathbf{x} = [x_1, \dots, x_N]^T$, where x_n is the precoded sample transmitted from n -th antenna in the BS. These variables together with all other essential variables used throughout this paper are listed in TABLE I at the very end of the manuscript.

As illustrated in Fig. 1, the effective DL and UL channels are generally cascades of transceiver frequency-responses and antenna mutual coupling at BS side, physical propagation channels, and transceiver responses at UE side. Thus, the effective DL channel \mathbf{H} and the effective UL channel \mathbf{G} can be written explicitly as

$$\begin{aligned} \mathbf{H} &= \mathbf{F}^{RX} \mathbf{P}^T \mathbf{M}^{TX} \mathbf{B}^{TX} \\ \mathbf{G} &= \mathbf{B}^{RX} \mathbf{M}^{RX} \mathbf{P} \mathbf{F}^{TX}, \end{aligned} \quad (2)$$

where $\mathbf{F} = \text{diag}(f_1, \dots, f_K)$ is the FR matrix of the UEs, $\mathbf{B} = \text{diag}(b_1, \dots, b_N)$ is the FR matrix of the BS, $\mathbf{M} \in \mathbb{C}^{N \times N}$ is the antenna mutual coupling matrix of the BS, and $\mathbf{P} \in \mathbb{C}^{N \times K}$ is the reciprocal physical channel, while the superscripts TX and RX specify the transmit and receive modes, respectively.

B. Channel Non-Reciprocity Problem

As outlined above, in TDD networks the BS obtains DL CSI based on the estimated UL channel, since DL and UL channels share the same spectrum and are assumed to be reciprocal within each channel

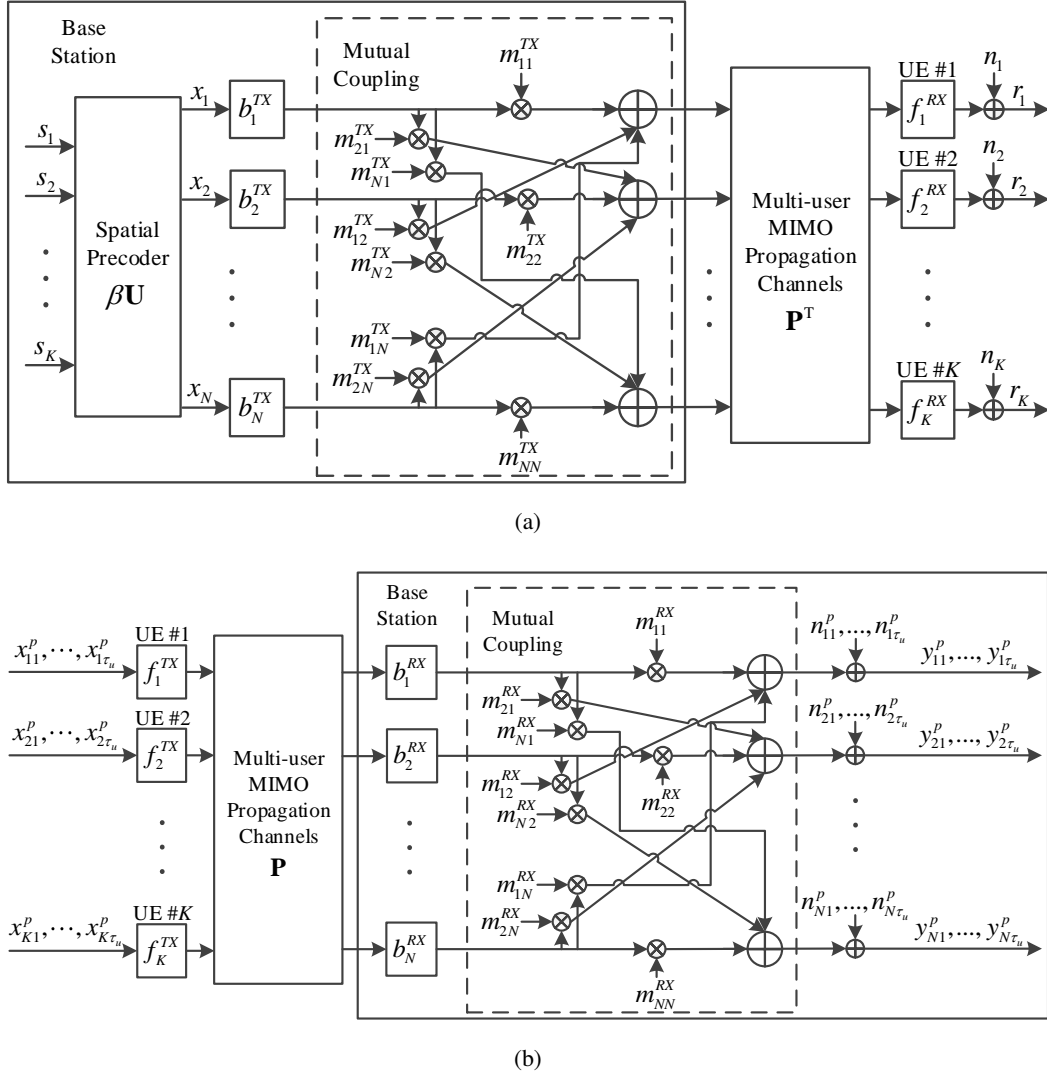


Fig. 1. Principal illustration of physical (a) DL and (b) UL transmissions and receptions including propagation channels, transceivers frequency responses and antenna mutual coupling in the devices.

coherence interval. The reciprocal nature applies, however, only to the physical propagation channel shown in Fig. 1. In addition to the physical channels, the effective channels also include the responses of electronics components used in the transmitting and receiving devices which results into the effective DL and UL channels expressed in (2).

Based on (2), the relation between the effective DL and UL channels can now be established as

$$\mathbf{H} = \mathbf{A}\mathbf{G}^T\mathbf{C}, \quad (3)$$

where the matrices \mathbf{A} and \mathbf{C} read

$$\begin{aligned}\mathbf{A} &= \mathbf{F}^{RX} (\mathbf{F}^{TX})^{-1} \\ \mathbf{C} &= (\mathbf{B}^{RX})^{-1} (\mathbf{M}^{RX})^{-1} \mathbf{M}^{TX} \mathbf{B}^{TX}.\end{aligned}\tag{4}$$

In (3) and (4), the matrices $\mathbf{A} \in \mathbb{C}^{K \times K}$ and $\mathbf{C} \in \mathbb{C}^{N \times N}$ are incorporating the effects of transceivers on non-reciprocity in UEs and BS, respectively. The matrix $\mathbf{A} = \text{diag}(a_1, \dots, a_K)$ is diagonal and can be written as $\mathbf{A} = \mathbf{I}_K + \mathbf{A}'$ where $\mathbf{A}' = \text{diag}(a'_1, \dots, a'_K)$ has i.i.d. $\mathcal{CN}(0, \sigma_A^2)$ elements and models the UE FR mismatch. On the other hand, \mathbf{C} which represents the overall BS transceiver non-reciprocity, including mutual coupling mismatch, is generally a full matrix and can be decomposed as $\mathbf{C} = \mathbf{I}_N + \mathbf{C}'$, where \mathbf{C}' has i.i.d. $\mathcal{CN}(0, \sigma_{C_d}^2)$ diagonal elements, and i.i.d. $\mathcal{CN}(0, \sigma_{C_{od}}^2)$ off-diagonal elements. In general, the channel non-reciprocity values vary very slowly with respect to the variations in the propagation channel and hence \mathbf{A} and \mathbf{C} can be assumed to remain constant over many channel coherence intervals. In above modeling, the level of reciprocity is controlled through the variance parameters σ_A^2 , $\sigma_{C_d}^2$, and $\sigma_{C_{od}}^2$. Furthermore, it can easily be deduced that the effective DL and UL channels are reciprocal if and only if the mismatch matrices satisfy $\mathbf{A}' = \mathbf{0}_K$ and $\mathbf{C}' = \mathbf{0}_N$.

C. Channel Estimation

To facilitate the channel estimation at BS, UEs simultaneously transmit mutually orthogonal UL pilot sequences of length τ_u such that $\mathbf{X}_p^H \mathbf{X}_p = \mathbf{I}_K$. To satisfy the orthogonality condition, the length of the UL pilot sequences has to be $\tau_u \geq K$.

To estimate the UL channels, the BS multiplies the received UL matrix in (1) with $(\mathbf{X}^p)^H$, which yields [7]

$$\mathbf{Y} = \mathbf{Y}^p (\mathbf{X}^p)^H = \sqrt{\tau_u \rho_u} \mathbf{G} + \mathbf{Q},\tag{5}$$

where the effective UL channel matrix \mathbf{G} is assumed to have independent columns, each having i.i.d. $\mathcal{CN}(0, 1)$ elements and $\mathbf{Q} \in \mathbb{C}^{N \times K}$ is the processed noise matrix with i.i.d. $\mathcal{CN}(0, 1)$ elements. Using minimum mean-square error (MMSE) channel estimator, the estimated effective DL channel $\hat{\mathbf{H}} \in \mathbb{C}^{K \times N}$

can be shown to be [25]

$$\hat{\mathbf{H}} = \hat{\mathbf{G}}^T = \frac{\tau_u \rho_u}{\tau_u \rho_u + 1} \mathbf{G}^T + \frac{\sqrt{\tau_u \rho_u}}{\tau_u \rho_u + 1} \mathbf{Q}^T, \quad (6)$$

where $\hat{\mathbf{G}} \in \mathbb{C}^{N \times K}$ denotes the estimated effective UL channel. Based on (6), the effective UL channel matrix \mathbf{G} can be decomposed as

$$\mathbf{G} = \hat{\mathbf{G}} + \mathbf{\mathcal{E}}^T = \hat{\mathbf{H}}^T + \mathbf{\mathcal{E}}^T, \quad (7)$$

where $\mathbf{\mathcal{E}} = [\varepsilon_1, \dots, \varepsilon_K]^T \in \mathbb{C}^{K \times N}$ accounts for the UL channel estimation error and has i.i.d. $\mathcal{CN}\left(0, \frac{1}{\tau_u \rho_u + 1}\right)$ elements. The estimated effective DL channel $\hat{\mathbf{H}}$ has i.i.d. $\mathcal{CN}\left(0, \frac{\tau_u \rho_u}{\tau_u \rho_u + 1}\right)$ elements and is independent of $\mathbf{\mathcal{E}}$.

Incorporating (7) in (3), we can next obtain the relation between the estimated and true effective DL channels as

$$\mathbf{H} = \mathbf{A} \mathbf{G}^T \mathbf{C} = \mathbf{A} \left(\hat{\mathbf{H}} + \mathbf{\mathcal{E}} \right) \mathbf{C}, \quad (8)$$

which summarizes the joint effects of two non-ideality sources, namely, UL channel estimation error and the channel non-reciprocity, on the effective DL channel estimation.

III. PERFORMANCE ANALYSIS UNDER NRC AND IMPERFECT CSI

In this section, we characterize the impacts of NRC and imperfect CSI on the performance of linearly precoded DL transmission in TDD multi-user massive MIMO systems. In this respect, we will derive analytical expressions for the received SINR and achievable rates for both ZF and MRT precoding schemes.

A. Downlink Received Signal Model and SINR

We express the linearly precoded DL transmit vector $\mathbf{x} \in \mathbb{C}^{N \times 1}$ as

$$\mathbf{x} = \beta \mathbf{U} \mathbf{s}, \quad (9)$$

where $\mathbf{U} = [\mathbf{u}_1, \dots, \mathbf{u}_K] \in \mathbb{C}^{N \times K}$ is the precoder matrix. The user data vector is denoted by $\mathbf{s} = [s_1, \dots, s_K]^T \in \mathbb{C}^{K \times 1}$, where the normalized power of each element is $\mathbb{E}[|s_k|^2] = 1$. The transmit power

normalization is achieved through β which constrains the total BS transmit power to 1, i.e.,

$$\mathbb{E}[\mathbf{x}^H \mathbf{x}] = 1. \quad (10)$$

In order to satisfy (10), β is chosen as [25]

$$\beta = \left(\sqrt{\mathbb{E}[\text{Tr}(\mathbf{U}^H \mathbf{U})]} \right)^{-1}. \quad (11)$$

Substituting next (9) in (2), the received DL data vector corresponding to all K UEs reads

$$\mathbf{r} = \beta \sqrt{\rho_d} \mathbf{H} \mathbf{U} \mathbf{s} + \mathbf{n}. \quad (12)$$

We express the effective DL channel matrix as $\mathbf{H} = [\mathbf{h}_1, \dots, \mathbf{h}_K]^T$, where \mathbf{h}_k^T is the effective DL channel towards the k -th UE. Then, based on (8) and (12), the received DL signal at the k -th UE can be expressed as

$$\begin{aligned} r_k &= \sqrt{\rho_d} \beta \mathbf{h}_k^T \mathbf{u}_k s_k + \sqrt{\rho_d} \sum_{i=1, i \neq k}^K \beta \mathbf{h}_k^T \mathbf{u}_i s_i + n_k \\ &= \sqrt{\rho_d} \beta a_k \left(\hat{\mathbf{h}}_k^T + \boldsymbol{\varepsilon}_k^T \right) \mathbf{C} \mathbf{u}_k s_k + \sqrt{\rho_d} \sum_{i=1, i \neq k}^K \beta a_k \left(\hat{\mathbf{h}}_k^T + \boldsymbol{\varepsilon}_k^T \right) \mathbf{C} \mathbf{u}_i s_i + n_k. \end{aligned} \quad (13)$$

Similar to [7], [22]–[24], we assume that UEs rely on the statistical properties of the channel to decode the received DL signal, i.e., the k -th UE uses only $\beta \mathbb{E}[\mathbf{h}_k^T \mathbf{u}_k]$ as the DL complex gain in the detection process. Therefore, the received signal at the k -th UE can be decomposed as

$$r_k = \underbrace{\sqrt{\rho_d} \beta \mathbb{E}[\mathbf{h}_k^T \mathbf{u}_k]}_{\text{useful signal}} s_k + z_k^{\text{SI}} + z_k^{\text{IUI}} + n_k, \quad (14)$$

where z_k^{SI} and z_k^{IUI} are the self-interference (SI) and inter-user interference (IUI), respectively, which can be explicitly expressed as

$$z_k^{\text{SI}} = \sqrt{\rho_d} \beta a_k \left(\hat{\mathbf{h}}_k^T + \boldsymbol{\varepsilon}_k^T \right) \mathbf{C} \mathbf{u}_k s_k - \sqrt{\rho_d} \beta \mathbb{E}[\mathbf{h}_k^T \mathbf{u}_k] s_k, \quad (15)$$

and

$$z_k^{\text{IUI}} = \sqrt{\rho_d} \sum_{i=1, i \neq k}^K \beta a_k \left(\hat{\mathbf{h}}_k^T + \boldsymbol{\varepsilon}_k^T \right) \mathbf{C} \mathbf{u}_i s_i. \quad (16)$$

Based on (14), the effective SINR for the k -th UE can be written as

$$\text{SINR} = \frac{\text{Var}(\sqrt{\rho_d} \beta \mathbb{E}[\mathbf{h}_k^T \mathbf{u}_k] s_k)}{\text{Var}(z_k^{\text{SI}}) + \text{Var}(z_k^{\text{IUI}}) + 1}, \quad (17)$$

where in defining (17) we used the fact that z_k^{SI} and z_k^{IUI} are uncorrelated.

In deriving capacity lower bounds, we follow the same approach as in [7], [26]. The total noise/interference term is uncorrelated with the useful signal whose entropy is upper-bounded with the entropy of Gaussian noise with equal variance. Moreover, since the total noise/interference term comprises many independent terms, especially for the case with large K , the probability density approaches to Gaussian density due to central limit theorem. Hence, a tight lower-bound on the achievable sum-rate can be expressed as

$$R = K \log_2 (1 + \text{SINR}). \quad (18)$$

Next, we derive analytical expressions for the SINR and achievable sum-rate R , given in (17) and (18), respectively, for two different linear precoding techniques, namely, ZF and MRT.

B. Zero-Forcing

For the ZF precoding scheme, the precoder matrix is constructed using the pseudo-inverse of the estimated effective DL channel matrix as [7]

$$\mathbf{U}^{\text{ZF}} = \hat{\mathbf{H}}^{\text{H}} \left(\hat{\mathbf{H}} \hat{\mathbf{H}}^{\text{H}} \right)^{-1}. \quad (19)$$

Next, based on (11), the normalization scalar β^{ZF} reads [7]

$$\beta^{\text{ZF}} = \left(\sqrt{\mathbb{E} \left[\text{Tr} \left(\left(\hat{\mathbf{H}} \hat{\mathbf{H}}^{\text{H}} \right)^{-1} \right) \right]} \right)^{-1} = \sqrt{\frac{(N - K) \tau_u \rho_u}{K (\tau_u \rho_u + 1)}}, \quad (20)$$

and based on (14), the useful signal for the detection at the k -th UE then reads

$$\sqrt{\rho_d} \beta^{\text{ZF}} \mathbb{E} \left[\mathbf{h}_k^{\text{T}} \mathbf{u}_k^{\text{ZF}} \right] s_k = \sqrt{\rho_d} \beta^{\text{ZF}} s_k. \quad (21)$$

By substituting (21) in (15) and (17), the effective SINR at the k -th UE for ZF precoding can be written as

$$\text{SINR}^{\text{ZF}} = \frac{N - K}{K} \times \frac{\tau_u \rho_u \rho_d}{I_{\text{RC}}^{\text{ZF}} + I_{\text{NRC}}^{\text{ZF}}}, \quad (22)$$

where $I_{\text{RC}}^{\text{ZF}} = \rho_d + \tau_u \rho_u + 1$ is the interference and noise power under reciprocal channel, whereas $I_{\text{NRC}}^{\text{ZF}}$ denotes the additional interference power due to NRC, which can be explicitly written as

$$I_{\text{NRC}}^{\text{ZF}} \approx \rho_d \left[\left(1 + \frac{N-K}{K} \tau_u \rho_u \right) \sigma_A^2 + (1 + \sigma_A^2) \left((\tau_u \rho_u + 1) \left[\left(1 + \frac{1}{K} \frac{\tau_u \rho_u}{\tau_u \rho_u + 1} \right) \sigma_{C_d}^2 + (N-1) \sigma_{C_{od}}^2 \right] \right) \right]. \quad (23)$$

Proof: See Appendix A.

Note that when the NRC parameters, namely σ_A^2 , $\sigma_{C_d}^2$, and $\sigma_{C_{od}}^2$, are set to 0, then $I_{\text{NRC}}^{\text{ZF}} = 0$ and (22) reduces to the SINR expression given in [7] for the ideal reciprocal case.

C. Maximum Ratio Transmission

For the MRT case, the precoder matrix is constructed as [25]

$$\mathbf{U}^{\text{MRT}} = \hat{\mathbf{H}}^{\text{H}}. \quad (24)$$

Therefore, based on (11), the normalization scalar β^{MRT} reads [25]

$$\beta^{\text{MRT}} = \left(\sqrt{\mathbb{E}[\text{Tr}(\hat{\mathbf{H}}\hat{\mathbf{H}}^{\text{H}})]} \right)^{-1} = \sqrt{\frac{\tau_u \rho_u + 1}{N K \tau_u \rho_u}}. \quad (25)$$

Based on (14), the useful signal for the detection at the k -th UE reads then

$$\sqrt{\rho_d} \beta^{\text{MRT}} \mathbb{E}[\mathbf{h}_k^{\text{T}} \mathbf{u}_k^{\text{MRT}}] s_k = \sqrt{\rho_d} \beta^{\text{MRT}} \frac{N \tau_u \rho_u}{\tau_u \rho_u + 1} s_k. \quad (26)$$

Stemming from this, the effective SINR at the k -th UE, defined in (17) can now be expressed as

$$\text{SINR}^{\text{MRT}} = \frac{N}{K} \times \frac{\tau_u \rho_u \rho_d}{I_{\text{RC}}^{\text{MRT}} + I_{\text{NRC}}^{\text{MRT}}}, \quad (27)$$

where $I_{\text{RC}}^{\text{MRT}} = (\rho_d + 1)(\tau_u \rho_u + 1)$ is the interference and noise power under reciprocal channel, whereas $I_{\text{NRC}}^{\text{MRT}}$ denotes the additional interference power due to NRC, and can be explicitly written as

$$I_{\text{NRC}}^{\text{MRT}} = \rho_d \left[\left(1 + \frac{N+K}{K} \tau_u \rho_u \right) \sigma_A^2 + (1 + \sigma_A^2) \left((\tau_u \rho_u + 1) \left[\left(1 + \frac{1}{K} \frac{\tau_u \rho_u}{\tau_u \rho_u + 1} \right) \sigma_{C_d}^2 + (N-1) \sigma_{C_{od}}^2 \right] \right) \right]. \quad (28)$$

Proof: See Appendix B.

Note again that when the NRC parameters, namely σ_A^2 , $\sigma_{C_d}^2$, and $\sigma_{C_{od}}^2$ are set to 0, then $I_{\text{NRC}}^{\text{MRT}} = 0$ and (27) reduces to the SINR expression for MRT precoding under ideal reciprocal case given in [7].

IV. ASYMPTOTIC RESULTS AND IMPLICATIONS

In this section, we will address several important implications stemming from the derived analytical SINR and achievable rate expressions. To this end, the asymptotic performance of ZF and MRT precoding schemes are first derived and compared. Then, the SINR degradation due to NRC is quantified and analyzed for both precoding techniques.

A. Asymptotic Performance for Large N

For growing N , the asymptotic SINR expressions of ZF and MRT under NRC, derived in the previous section, can be shown to be identical and have the following saturation value of the form

$$\lim_{N \rightarrow \infty} \text{SINR}^{\text{ZF}} = \lim_{N \rightarrow \infty} \text{SINR}^{\text{MRT}} = \frac{1}{\sigma_A^2 + K \left(1 + \sigma_A^2\right)^{\frac{\tau_u \rho_u + 1}{\tau_u \rho_u}} \sigma_{C_{od}}^2}. \quad (29)$$

Note that the number of mismatched transceiver chains increases with the number of antennas which in turn increases the level of interference power due to NRC. Thus, the system is subject to additional interference which cannot be suppressed by NRC-blind spatial precoders. Therefore, for massive MIMO links with practical non-reciprocal transceivers, the advantage of ZF over MRT in terms of IUI suppression, and hence in SINR performance, reduces or even vanishes with increasing number of antennas and transceiver chains. This will be illustrated also through numerical examples in Section V.

We next quantify the relative achievable rate performance under ZF and MRT precoding schemes with the ratio $R^{\text{ZF}}/R^{\text{MRT}}$, where R^{ZF} and R^{MRT} are obtained by substituting (22) and (27) into (18), respectively. The asymptotic behavior of this relative achievable rate performance for large number of antennas can be shown to read

$$\lim_{N \rightarrow \infty} \frac{R^{\text{ZF}}}{R^{\text{MRT}}} = \lim_{N \rightarrow \infty} \frac{\log_2(1 + \text{SINR}^{\text{ZF}})}{\log_2(1 + \text{SINR}^{\text{MRT}})} = 1. \quad (30)$$

Based on above, the asymptotic behavior of relative achievable rate under NRC is similar to the reciprocal case presented in [7]. However, the implications of these two results are largely different. More specifically, (30) establishes that the achievable rates for both precoders have identical but finite saturation levels in the presence of NRC. On the other hand, for ideal reciprocal channel, this asymptotic result implies that

the rate grows without bound for both precoding schemes. Also this will be illustrated through numerical examples in Section V.

B. Non-Asymptotic Comparison of SINR Performance

We next pursue a non-asymptotic comparison of the achievable SINRs between ZF and MRT precoding schemes under NRC. Building on the SINR expressions in (22) and (27), the following relation can be deduced

$$\frac{\text{SINR}^{\text{ZF}}}{\text{SINR}^{\text{MRT}}} = 1 + \frac{K}{N} (\text{SINR}^{\text{ZF}} - 1) + \left(1 - \frac{K}{N}\right) \frac{2\rho_d\tau_u\rho_u\sigma_A^2}{\rho_d + \tau_u\rho_u + 1 + I_{\text{NRC}}^{\text{ZF}}}. \quad (31)$$

Based on above, since $N > K$, ZF outperforms MRT in the achievable SINR, and consequently in the capacity lower bound, if $\text{SINR}^{\text{ZF}} \geq 1$. In the special case of $N \rightarrow \infty$, the ratio in (31) tends towards one, conforming with the previous asymptotic results.

In practical scenarios where channel non-reciprocity level is not overly high, and considering the high SNR region with reasonably good UL channel estimation accuracy, SINR is always greater than one for ZF precoding scheme. Therefore, in high SNR region, (31) shows that ZF has better non-asymptotic performance compared to MRT. On the other hand, in low SNR region, performance of both systems are limited by noise and the difference becomes negligible.

C. SINR Degradation at Large SNR

In order to next quantify the SINR degradation under non-reciprocal channels with respect to ideal reciprocal channel, we define the following metric

$$\alpha = \frac{\text{SINR}_{\text{RC}} - \text{SINR}_{\text{NRC}}}{\text{SINR}_{\text{RC}}}. \quad (32)$$

In (32), SINR_{NRC} stands for the SINR under non-reciprocal channels calculated based on (17) and for which closed-form analytic expressions are given in (22) and (27) under ZF and MRT precoding schemes, respectively. Furthermore, SINR_{RC} denotes the SINR under reciprocal channel for which closed-form expressions can be obtained under ZF and MRT precoding schemes from [7], or by setting the NRC

parameters to 0 in (22) and (27), respectively. To compare the relative SINR degradation of ZF and MRT precoding schemes, we also define the ratio $\alpha^{\text{ZF/MRT}} = \frac{\alpha^{\text{ZF}}}{\alpha^{\text{MRT}}}$, where α^{ZF} and α^{MRT} are calculated using (32) with their corresponding SINR_{NRC} and SINR_{RC} expressions for ZF and MRT precoding schemes, respectively.

At high SNR region, when $\rho_d \gg 1$, this ratio can be shown to read

$$\lim_{\rho_d \rightarrow \infty} \frac{\alpha^{\text{ZF}}}{\alpha^{\text{MRT}}} \triangleq \alpha_{\infty}^{\text{ZF/MRT}} = \frac{I_0 + \tau_u \rho_u I_{\text{NRC}}^{\text{ZF}} / \rho_d}{I_0 + 2\tau_u \rho_u \sigma_A^2}, \quad (33)$$

where $I_0 = (2\tau_u \rho_u \sigma_A^2 + I_{\text{NRC}}^{\text{ZF}} / \rho_d + 1) I_{\text{NRC}}^{\text{ZF}} / \rho_d$. From (33), it can be seen that $\alpha_{\infty}^{\text{ZF/MRT}} > 1$ when $I_{\text{NRC}}^{\text{ZF}} / \rho_d > 2\sigma_A^2$. Note that based on (23), for practical setting of $\tau_u \geq K$, this holds when

$$\rho_u > \frac{1}{N - K}. \quad (34)$$

Hence, in general, under practical settings of $N \gg K$, the inequality given in (34) is satisfied, implying that ZF precoding is more sensitive to channel non-reciprocity, that is, the SINR degradation due to NRC is higher for ZF than for MRT, at large SNR.

V. NUMERICAL RESULTS AND DISCUSSIONS

In this section, we will provide extensive numerical evaluations of the derived analytical SINR and achievable rate expressions for precoded multi-user massive MIMO system with imperfect CSI and channel non-reciprocity. We will also study the behavior of the system spectral efficiency, formally defined as [7]

$$\eta_s = \left(1 - \frac{\tau_u}{T}\right) R = \left(1 - \frac{\tau_u}{T}\right) K \log_2 (1 + \text{SINR}), \quad (35)$$

where T is the number of symbols in each channel coherence interval. Finally, we will discuss and summarize the novel findings of this work based on the derived analytical expressions and obtained numerical results.

A. Obtained Numerical Results

The baseline simulation scenario consists of a BS which is equipped with $N = 100$ antenna elements and $K = 10$ single-antenna UEs that are served simultaneously through either ZF or MRT precoding. We

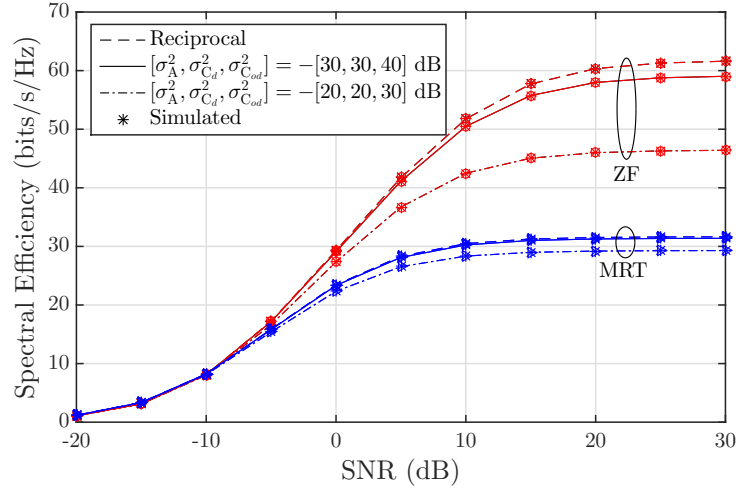


Fig. 2. Spectral efficiency vs. DL SNR (ρ_d) for $N = 100$, $K = 10$, $\tau_u = K$, $\rho_u = 0$ dB, $T = 196$. In obtaining solid and dash-dot curves, derived analytical expression in (22) and (27) are plugged into (35) for ZF and MRT precoding, respectively.

assume that the channel coherence interval is 1ms, which corresponds to one radio sub-frame in 3GPP LTE/LTE-Advanced radio network [27] and specifically contains $T = 196$ symbols, while the number of UL pilots sent by each UE is always equal to the number of scheduled UEs, i.e., $\tau_u = K$. The UL SNR is set to $\rho_u = 0$ dB, while DL SNR is chosen to be $\rho_d = 20$ dB. These are the baseline simulation settings, while some of the parameter values are also varied in the evaluations.

In Fig. 2 and Fig. 3, the spectral efficiency and relative SINR degradation curves are plotted against DL SNR for indicated NRC parameter settings. In obtaining solid and dash-dot curves, the derived analytical expressions in (22) and (27) are plugged into (35) for ZF and MRT precoding schemes, respectively. In addition to that, simulated curves are obtained via extensive empirical SINR and corresponding spectral efficiency evaluations which are averaged over 1000 independent channel and NRC realizations. As can be seen in Fig. 2, the analytical and simulated curves for both ZF and MRT have a perfect match showing the accuracy of derived expressions. Thus, in the continuation we will use only the derived analytical expressions. As illustrated in Fig. 2 and Fig. 3, in low SNR region, the effect of channel non-reciprocity on both precoding schemes is negligible as the performance is limited by noise. On the other hand,

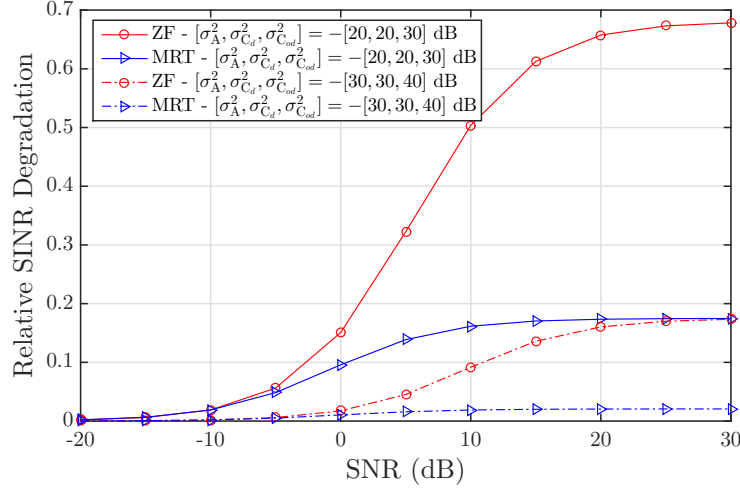


Fig. 3. Relative SINR degradation (α) vs. DL SNR (ρ_d) for $N = 100$, $K = 10$, $\tau_u = K$, $\rho_u = 0$ dB, $T = 196$.

in high SNR region, there is an observable performance loss, especially for ZF precoding scheme. For instance, from Fig. 2 we observe that for ZF at $\rho_d = 15$ dB, when the system is subject to practical NRC parameter settings of $\sigma_A^2 = -20$ dB, $\sigma_{C_d}^2 = -20$ dB, and $\sigma_{C_{od}}^2 = -30$ dB, the spectral efficiency has decreased 14 bits/s/Hz compared to the reciprocal channel case. For the same settings, the degradation for MRT precoding scheme is only 2 bits/s/Hz showing that MRT is less sensitive to channel non-reciprocity compared to ZF.

Based on the derived expressions in (23) and (28), the contributions of $\sigma_{C_{od}}^2$, σ_A^2 , and $\sigma_{C_d}^2$ to the total received interference are proportional to NK , N/K , and K , respectively. In typical settings with $N \gg K$ (which is also the case with $N = 100$ and $K = 10$), these cofactors satisfy the relation $NK > N/K > K$, and hence we have the highest sensitivity with respect to $\sigma_{C_{od}}^2$ and the lowest sensitivity with respect to $\sigma_{C_d}^2$. In order to demonstrate this effect, in Fig. 4, the relative SINR degradation is plotted against different levels of each channel non-reciprocity parameter individually, i.e., when the level of one channel non-reciprocity parameter is varied, all other channel non-reciprocity parameter values are deliberately set to 0. As expected, the obtained results show that both ZF and MRT precoding schemes are most sensitive to the power levels of off-diagonal elements of the BS non-reciprocity matrix. For instance, for the case with

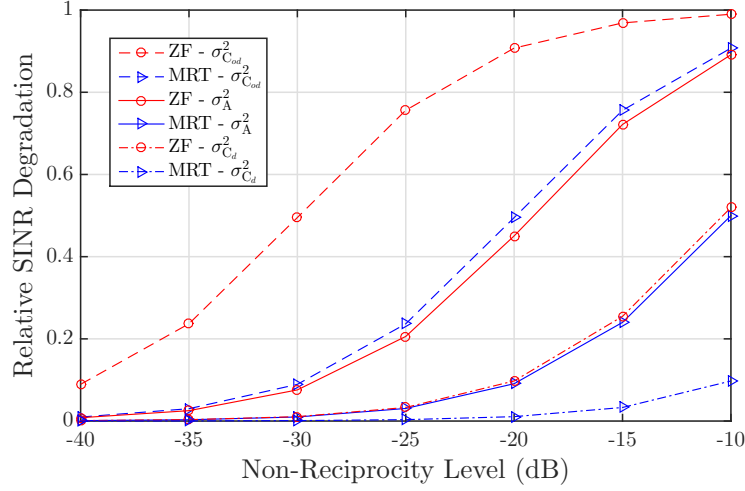


Fig. 4. Relative SINR degradation (α) vs. the level of an individual non-reciprocity source (with others being zero, i.e., ideal) for $N = 100$, $K = 10$, $\rho_d = 20$, $\tau_u = K$, $\rho_u = 0$ dB, $T = 196$.

$\sigma_{C_{od}}^2 = -25$ dB, the SINR degradation is approximately 80% for ZF and 20% for MRT. The sensitivity with respect to UE side FR mismatch is also considerably high especially for ZF precoding. For instance, the SINR degradation increases from 20% to 43%, when σ_A^2 is increased from -25 dB to -20 dB. For the same levels, the SINR degradation of MRT increases from 3% to 10%, which can also be considered a significant loss. Finally, as expected, SINR degradation is the least sensitive against the power levels of the diagonal entries of BS side non-reciprocity matrix. It is seen that ZF precoded system starts to have observable performance loss for values of $\sigma_{C_d}^2 > -20$ dB, whereas for MRT precoded system this threshold value is as high as $\sigma_{C_d}^2 > -10$ dB.

The derived analytical expressions for the asymptotic achievable performance in Section IV indicate two new results and findings which differ from the ordinary reciprocal case; 1) there is a saturation level for both MRT and ZF precoding schemes, and 2) this saturation level is identical for both precoding techniques. In order to verify and demonstrate this behavior, the spectral efficiency is plotted against the number of BS antennas in Fig. 5. It can be clearly seen that both MRT and ZF spectral efficiency curves saturate towards the levels predicted by the derived analytical expression in (29). As discussed earlier

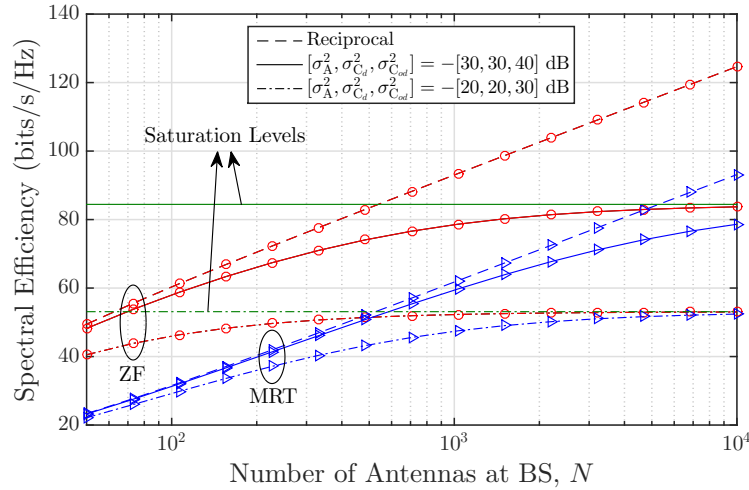


Fig. 5. Spectral efficiency vs. the number of antennas at BS (N) for $K = 10$, $\rho_d = 20$, $\tau_u = K$, $\rho_u = 0$ dB, $T = 196$. Saturation levels based on (31) are plotted in green horizontal lines for indicated NRC parameter settings.

in Section IV-A, the system is subject to increasing levels of interference with increasing number of antennas and corresponding mismatched chains. Since this interference cannot be suppressed by NRC-blind spatial precoders, in contrast to the reciprocal case, the advantage of ZF over MRT in terms of inter-user interference suppression and higher achievable rates gradually vanishes.

Fig. 6 shows the impact of channel non-reciprocity on the optimal number of UEs, K_{opt} , to achieve maximal spectral efficiency for two different values of DL SNR, namely, $\rho_d = 20$ dB, 0 dB. This optimum number is achieved by evaluating (18) for all the values of K in the range $N \geq K \geq 1$, and choosing the one which maximizes the spectral efficiency. The optimal number of UEs drops for both precoding techniques as the system is subject to increasing interference power with increasing non-reciprocity levels. For low SNR regime (0 dB), this drop is not severe as the thermal noise has dominating impact on system performance. However, in high SNR regime (20 dB), there is a significant drop in the optimal number of UEs for ZF, even for moderate channel non-reciprocity levels, say -30 dB $< \sigma_A^2 < -20$ dB, whereas for MRT there is a drop only at fairly severe non-reciprocity levels, e.g., $\sigma_A^2 > -15$ dB. An interesting and new observation is that, in contrast to high SNR regime behavior in the ordinary

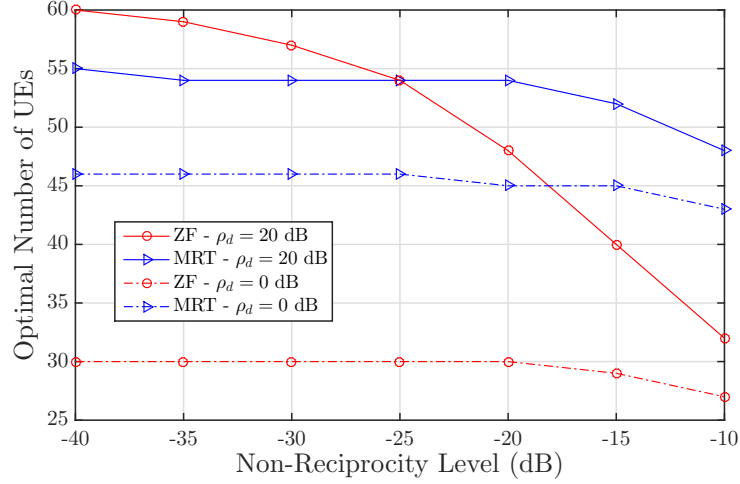


Fig. 6. Optimal number of UEs to maximize system spectral efficiency vs. non-reciprocity level ($\sigma_{C_d}^2 = \sigma_A^2 = \text{NRC level}$, while $\sigma_{C_{od}}^2 = \text{NRC level} - 10$ dB) for $N = 100$, $K = 10$, $\tau_u = K$, $\rho_u = 0$ dB, $T = 196$.

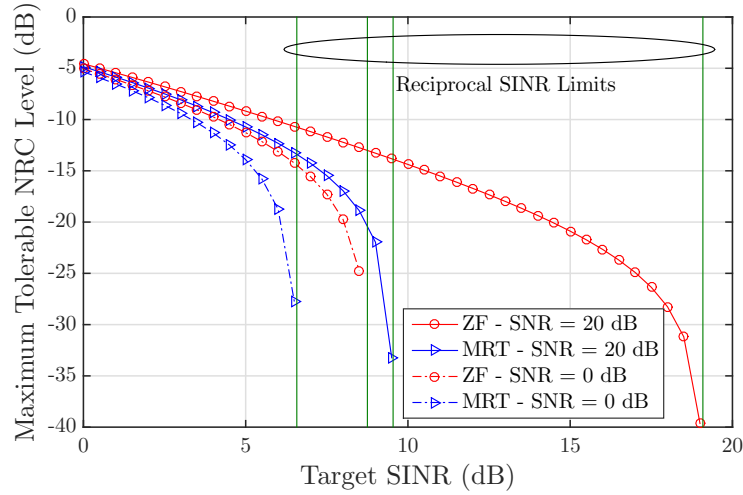


Fig. 7. Maximum tolerable non-reciprocity level vs. target SINR ($\sigma_{C_d}^2 = \sigma_A^2 = \text{NRC level}$, while $\sigma_{C_{od}}^2 = \text{NRC level} - 10$ dB) for $N = 100$, $K = 10$, $\tau_u = K$, $\rho_u = 0$ dB, $T = 196$.

reciprocal case, the optimal number of users for MRT is higher than that of ZF under moderate channel non-reciprocity levels.

In Fig. 7, based on the derived closed-form expressions for SINR in (22) and (27), the maximum

tolerable NRC level is evaluated as a function of target SINR in the UE side, for two example values of DL SNR, namely, $\rho_d = 20$ dB, 0 dB. Based on the obtained results, in order to have SINR at UEs for example equal to 15 dB, the maximum NRC level which can be tolerated is around -20 dB. This demonstrates the value and applicability of the provided analytical results, in for example evaluating and extracting the required NRC calibration levels such that given DL transmission performance can be achieved.

B. Summary of New Findings

In this section, we shortly summarize the novel scientific findings and concrete contributions of this work compared to the existing literature regarding the performance of massive MIMO systems with practical mismatched transceiver chains:

- 1) Based on (31), for the same channel non-reciprocity levels, ZF outperforms MRT in terms of the SINR and achievable rates. However, based on derived expressions in (33), the performance difference between the two precoding techniques starts to reduce as the level of channel non-reciprocity grows.
- 2) In previous literature, UE side FR mismatch was assumed to have negligible effect on the total received interference [18]. However, this is only true when DL pilots are used to further enhance the detection at UEs. On the other hand, when UEs rely only on statistical channel properties, the UE side FR mismatch has significant contribution to total received interference power. As can be inferred from derived expressions in (23) and (28), for both precoding techniques, this contribution scales with N/K which is typically a large number under the massive MIMO framework of $N \gg K$.
- 3) The received SINR and achievable rates saturate at a finite value asymptotically with increasing N . This is different from the ideal reciprocal case where adding more antennas decreases the residual IUI and hence increases the spatial separation of UEs. This phenomenon is due to the additional interference introduced by adding more mismatched transceivers with increasing N .

- 4) Optimal number of scheduled users under MRT is higher than that with ZF when considering moderate channel non-reciprocity levels. This is in contrast to the ideal reciprocal channel case where the optimal number of scheduled users is always higher for ZF precoding scheme [7].

VI. CONCLUSION

Closed-form performance analysis of TDD-based linearly precoded massive MIMO DL system under channel non-reciprocity and imperfect CSI was carried out in this manuscript. The derived analytical SINR and achievable rate expressions show that in general ZF precoding scheme is more sensitive to NRC levels compared to MRT. The derived analytical expressions also show that under practical NRC parameter settings, the performance gap between the two precoders decreases significantly. Moreover, in contrast to ideal reciprocal case, it was shown that the SINR and achievable rate saturate to a finite level with increasing antenna array size. Overall, the derived analytical expressions provide useful tools in dimensioning and designing practical massive MIMO systems with given performance targets, e.g., choosing the appropriate precoder based on performance-complexity trade-off, deciding the number of active antenna elements, and/or the needed frequency and accuracy of adopted NRC calibration schemes.

APPENDIX

In order to calculate SINR in (17), we need to compute the powers of the different interference terms, namely, z_k^{SI} and z_k^{IUI} , under ZF and MRT precoding schemes. In the continuation, the following properties and approximations are used.

- *Property 1:*

$$\sum_{l=1}^N \sum_{q=1}^N \sum_{m=1}^N \sum_{r=1}^N \mathbb{E}[c'_{lq} c'^*_{mr}] = \sum_{l=1}^N \sum_{q=1}^N \mathbb{E}[c'_{lq} c'^*_{lq}], \quad (36)$$

since $\mathbb{E}[c'_{lq} c'^*_{mr}] = 0$ for $l \neq m$ and/or $q \neq r$.

- *Property 2:*

$$\sum_{l=1}^N \sum_{m=1}^N \mathbb{E}[\epsilon_{kl} \epsilon^*_{km}] = \sum_{l=1}^N \mathbb{E}[\epsilon_{kl} \epsilon^*_{kl}], \quad (37)$$

since $\mathbb{E}[\epsilon_{kl} \epsilon^*_{km}] = 0$ for $l \neq m$.

- *Property 3:*

$$\sum_{l=1}^N \sum_{m=1}^N \mathbb{E} \left[u_{lk}^{\text{ZF}} u_{mk}^{\text{ZF}*} \right] = \sum_{l=1}^N \mathbb{E} \left[u_{lk}^{\text{ZF}} u_{lk}^{\text{ZF}*} \right], \quad (38)$$

since $\mathbb{E} \left[u_{lk}^{\text{ZF}} u_{mk}^{\text{ZF}*} \right] = 0$ for $l \neq m$.

- *Property 4:*

$$\sum_{l=1}^N \sum_{n=1}^N \mathbb{E} \left[\hat{h}_{kl} \hat{h}_{km}^* \right] = \sum_{l=1}^N \mathbb{E} \left[\hat{h}_{kl} \hat{h}_{kl}^* \right], \quad (39)$$

since $\mathbb{E} \left[\hat{h}_{kl} \hat{h}_{km}^* \right] = 0$ for $l \neq m$.

- *Approximation 1:* For mathematical tractability, we employ the following approximation [20]

$$u_{li}^{\text{ZF}} \approx \frac{\hat{h}_{il}^*}{v}, \quad (40)$$

where v is a constant that is chosen to satisfy $\mathbb{E} \left[|u_{li}^{\text{ZF}}|^2 \right] = \frac{1}{NK} \mathbb{E} \left[\text{Tr} \left(\mathbf{U}^{\text{ZFH}} \mathbf{U}^{\text{ZF}} \right) \right]$, and hence can be expressed as

$$v = \sqrt{N(N-K)} \frac{\tau_u \rho_u}{\tau_u \rho_u + 1}. \quad (41)$$

A. Interference Powers under ZF Precoding

Based on (15), (19), and (21), the power of self interference can be expressed as

$$\begin{aligned} \text{Var} \left(z_k^{\text{SI,ZF}} \right) &= \mathbb{E} \left[\left| \sqrt{\rho_d} \beta^{\text{ZF}} a_k \left(\hat{\mathbf{h}}_k^{\text{T}} + \boldsymbol{\varepsilon}_k^{\text{T}} \right) \mathbf{C} \mathbf{u}_k^{\text{ZF}} s_k - \sqrt{\rho_d} \beta^{\text{ZF}} s_k \right|^2 \right] \\ &= \rho_d \left(\beta^{\text{ZF}} \right)^2 \left(\underbrace{\mathbb{E} \left[|a'_k s_k|^2 \right]}_{t_1^{\text{SI,ZF}}} + \underbrace{\mathbb{E} \left[|a_k \hat{\mathbf{h}}_k^{\text{T}} \mathbf{C}' \mathbf{u}_k^{\text{ZF}} s_k|^2 \right]}_{t_2^{\text{SI,ZF}}} + \underbrace{\mathbb{E} \left[|a_k \boldsymbol{\varepsilon}_k^{\text{T}} \mathbf{C} \mathbf{u}_k^{\text{ZF}} s_k|^2 \right]}_{t_3^{\text{SI,ZF}}} \right). \end{aligned} \quad (42)$$

Next we will derive analytical expressions for the terms $t_1^{\text{SI,ZF}}$, $t_2^{\text{SI,ZF}}$, and $t_3^{\text{SI,ZF}}$. Starting with $t_1^{\text{SI,ZF}}$, we obtain

$$t_1^{\text{SI,ZF}} = \mathbb{E} \left[|a'_k s_k|^2 \right] = \mathbb{E} \left[|a'_k|^2 \right] \mathbb{E} \left[|s_k|^2 \right] = \sigma_{\text{A}}^2. \quad (43)$$

Following that, $t_2^{\text{SI,ZF}}$ can be expressed as

$$\begin{aligned}
t_2^{\text{SI,ZF}} &= \mathbb{E} \left[\left| a_k \hat{\mathbf{h}}_k^T \mathbf{C}' \mathbf{u}_k^{\text{ZF}} s_k \right|^2 \right] = \mathbb{E} \left[\left(a_k \sum_{l=1}^N \sum_{q=1}^N \hat{h}_{kl} c'_{lq} u_{qk}^{\text{ZF}} s_k \right) \left(a_k \sum_{m=1}^N \sum_{r=1}^N \hat{h}_{km} c'_{mr} u_{rk}^{\text{ZF}} s_k \right)^* \right] \\
&\approx \frac{1}{N(N-K)} \mathbb{E}[|a_k|^2] \mathbb{E}[|s_k|^2] \sum_{l=1}^N \sum_{q=1}^N \sum_{m=1}^N \sum_{r=1}^N \mathbb{E} \left[\frac{\hat{h}_{kl} \hat{h}_{kq}^* \hat{h}_{km}^* \hat{h}_{kr}}{\left(\frac{\tau_u \rho_u}{\tau_u \rho_u + 1} \right)^2} \right] \mathbb{E}[c'_{lq} c'_{mr}^*] \\
&= \frac{1 + \sigma_A^2}{N(N-K) \left(\frac{\tau_u \rho_u}{\tau_u \rho_u + 1} \right)^2} \sum_{l=1}^N \sum_{q=1}^N \mathbb{E} \left[\hat{h}_{kl} \hat{h}_{kl}^* \hat{h}_{kq} \hat{h}_{kq}^* \right] \mathbb{E}[c'_{lq} c'_{lq}^*] \\
&= \frac{1 + \sigma_A^2}{N-K} (2\sigma_{C_d}^2 + (N-1)\sigma_{C_{od}}^2).
\end{aligned} \tag{44}$$

In above, we used the Approximation 1 when obtaining the expression on the second line, whereas third line is obtained using Property 1.

Finally, the term $t_3^{\text{SI,ZF}}$ can be expressed as

$$\begin{aligned}
t_3^{\text{SI,ZF}} &= \mathbb{E} \left[\left| a_k \boldsymbol{\epsilon}_k^T \mathbf{C} \mathbf{u}_k^{\text{ZF}} s_k \right|^2 \right] = \mathbb{E} \left[\left(a_k \sum_{l=1}^N \sum_{q=1}^N \epsilon_{kl} c_{lq} u_{qk}^{\text{ZF}} s_k \right) \left(a_k \sum_{m=1}^N \sum_{r=1}^N \epsilon_{km} c_{mr} u_{rk}^{\text{ZF}} s_k \right)^* \right] \\
&= (1 + \sigma_A^2) \sum_{l=1}^N \sum_{q=1}^N \mathbb{E}[\epsilon_{kl} \epsilon_{kl}^*] \mathbb{E}[c_{lq} c_{lq}^*] \mathbb{E}[u_{qk}^{\text{ZF}} u_{qk}^{\text{ZF}*}] \\
&= \frac{1 + \sigma_A^2}{\tau_u \rho_u + 1} \left(\sum_{l=1}^N \mathbb{E}[|c_{ll}|^2] + \sum_{l=1}^N \sum_{q=1, q \neq l}^N \mathbb{E}[|c_{lq}|^2] \right) \left(\frac{1}{NK} \mathbb{E}[\text{Tr}(\mathbf{U}^{\text{ZFH}} \mathbf{U}^{\text{ZF}})] \right) \\
&= \frac{1 + \sigma_A^2}{K(\beta^{\text{ZF}})^2 (\tau_u \rho_u + 1)} (1 + \sigma_{C_d}^2 + (N-1)\sigma_{C_{od}}^2).
\end{aligned} \tag{45}$$

In obtaining the second line, we used Property 2 and Property 3.

The final expression for the variance of self interference in the ZF precoded system can be written, by substituting (20), (43), (44), and (45) in (42), which yields

$$\begin{aligned}
\text{Var} \left(z_k^{\text{SI,ZF}} \right) &\approx \rho_d \frac{(N-K) \tau_u \rho_u}{K (\tau_u \rho_u + 1)} \sigma_A^2 + \rho_d \frac{\tau_u \rho_u (1 + \sigma_A^2)}{K (\tau_u \rho_u + 1)} (2\sigma_{C_d}^2 + (N-1)\sigma_{C_{od}}^2) \\
&\quad + \rho_d \frac{1 + \sigma_A^2}{K (\tau_u \rho_u + 1)} (1 + \sigma_{C_d}^2 + (N-1)\sigma_{C_{od}}^2).
\end{aligned} \tag{46}$$

Similarly, based on (16), the power of the IUI under ZF precoding scheme can be written as

$$\begin{aligned} \text{Var} \left(z_k^{\text{IUI,ZF}} \right) &= \mathbb{E} \left[\left| \sqrt{\rho_d} \sum_{i=1, i \neq k}^K \beta^{\text{ZF}} a_k \left(\hat{\mathbf{h}}_k^T + \boldsymbol{\varepsilon}_k^T \right) \mathbf{C} \mathbf{u}_i^{\text{ZF}} s_i \right|^2 \right] \\ &= (K-1) \rho_d (\beta^{\text{ZF}})^2 \left(\underbrace{\mathbb{E} \left[\left| a_k \hat{\mathbf{h}}_k^T \mathbf{C}' \mathbf{u}_i^{\text{ZF}} s_i \right|^2 \right]}_{t_1^{\text{IUI,ZF}}} + \underbrace{\mathbb{E} \left[\left| a_k \boldsymbol{\varepsilon}_k^T \mathbf{C} \mathbf{u}_i^{\text{ZF}} s_i \right|^2 \right]}_{t_2^{\text{IUI,ZF}}} \right). \end{aligned} \quad (47)$$

Next, we will derive analytical expressions for the terms $t_1^{\text{IUI,ZF}}$ and $t_2^{\text{IUI,ZF}}$. Starting with $t_1^{\text{IUI,ZF}}$, we obtain

$$\begin{aligned} t_1^{\text{IUI,ZF}} &= \mathbb{E} \left[\left| a_k \hat{\mathbf{h}}_k^T \mathbf{C}' \mathbf{u}_i^{\text{ZF}} s_i \right|^2 \right]_{i \neq k} \\ &\approx \frac{1 + \sigma_A^2}{N(N-K) \left(\frac{\tau_u \rho_u}{\tau_u \rho_u + 1} \right)^2} \sum_{l=1}^N \sum_{q=1}^N \mathbb{E} \left[\hat{h}_{kl} \hat{h}_{kl}^* \right] \mathbb{E} \left[c'_{lq} c'_{lq} \right] \mathbb{E} \left[\hat{h}_{iq} \hat{h}_{iq}^* \right]_{i \neq k} \\ &= \frac{1 + \sigma_A^2}{N-K} \left(\sigma_{C_d}^2 + (N-1) \sigma_{C_{od}}^2 \right). \end{aligned} \quad (48)$$

In above, we used the Approximation 1 and Property 1 when obtaining the expression on the second line.

Then, $t_2^{\text{IUI,ZF}}$ can be expressed as

$$\begin{aligned} t_2^{\text{IUI,ZF}} &= \mathbb{E} \left[\left| a_k \boldsymbol{\varepsilon}_k^T \mathbf{C} \mathbf{u}_i^{\text{ZF}} s_i \right|^2 \right]_{i \neq k} = \mathbb{E} \left[\left(a_k \sum_{l=1}^N \sum_{q=1}^N \epsilon_{kl} c_{lq} u_{qi}^{\text{ZF}} s_i \right) \left(a_k \sum_{m=1}^N \sum_{r=1}^N \epsilon_{km} c_{mr} u_{ri}^{\text{ZF}} s_i \right)^* \right] \\ &= \frac{1 + \sigma_A^2}{K (\beta^{\text{ZF}})^2 (\tau_u \rho_u + 1)} \left(1 + \sigma_{C_d}^2 + (N-1) \sigma_{C_{od}}^2 \right). \end{aligned} \quad (49)$$

In obtaining the second line, we used Property 2 and Property 3.

The final expression for the IUI power under ZF precoding scheme can be obtained by plugging (48) and (49) into (47), which yields

$$\begin{aligned} \text{Var} \left(z_k^{\text{IUI,ZF}} \right) &\approx \rho_d \frac{(K-1) \tau_u \rho_u (1 + \sigma_A^2)}{K (\tau_u \rho_u + 1)} \left(\sigma_{C_d}^2 + (N-1) \sigma_{C_{od}}^2 \right) \\ &\quad + \rho_d \frac{(K-1) (1 + \sigma_A^2)}{K (\tau_u \rho_u + 1)} \left(1 + \sigma_{C_d}^2 + (N-1) \sigma_{C_{od}}^2 \right). \end{aligned} \quad (50)$$

The total interference power can be obtained by summing $\text{Var} \left(z_k^{\text{SI,ZF}} \right)$ and $\text{Var} \left(z_k^{\text{IUI,ZF}} \right)$ from (46) and (50), respectively. Then, it is straightforward to re-arrange the terms and express the total interference power as $I_{\text{RC}}^{\text{ZF}} + I_{\text{NRC}}^{\text{ZF}}$ after which we reach the SINR expression presented in (22).

B. Interference Powers under MRT Precoding

Based on (15), (24), and (26), the power of self interference under MRT precoding scheme can be expressed as

$$\begin{aligned}
\text{Var} \left(z_k^{\text{SI,MRT}} \right) &= \mathbb{E} \left[\left| \sqrt{\rho_d} \beta^{\text{MRT}} a_k \left(\hat{\mathbf{h}}_k^T + \boldsymbol{\varepsilon}_k^T \right) \mathbf{C} \mathbf{u}_k^{\text{MRT}} s_k - \sqrt{\rho_d} \beta^{\text{MRT}} \frac{N \tau_u \rho_u}{\tau_u \rho_u + 1} s_k \right|^2 \right] \\
&= \rho_d (\beta^{\text{MRT}})^2 \left(\mathbb{E} \left[\left| a_k \hat{\mathbf{h}}_k^T \hat{\mathbf{h}}_k^* s_k \right|^2 \right] + \mathbb{E} \left[\left| a_k \hat{\mathbf{h}}_k^T \mathbf{C}' \hat{\mathbf{h}}_k^* s_k \right|^2 \right] + \mathbb{E} \left[\left| a_k \boldsymbol{\varepsilon}_k^T \mathbf{C} \hat{\mathbf{h}}_k^* s_k \right|^2 \right] \right. \\
&\quad \left. + \mathbb{E} \left[\left| \frac{N \tau_u \rho_u}{\tau_u \rho_u + 1} s_k \right|^2 \right] - \mathbb{E} \left[\hat{\mathbf{h}}_k^T \mathbf{u}_k^{\text{MRT}} s_k \left(\frac{N \tau_u \rho_u}{\tau_u \rho_u + 1} s_k \right)^* \right] - \mathbb{E} \left[\left(\hat{\mathbf{h}}_k^T \mathbf{u}_k^{\text{MRT}} s_k \right)^* \frac{N \tau_u \rho_u}{\tau_u \rho_u + 1} s_k \right] \right) \\
&= \rho_d (\beta^{\text{MRT}})^2 \left(\underbrace{\mathbb{E} \left[\left| a_k \hat{\mathbf{h}}_k^T \hat{\mathbf{h}}_k^* s_k \right|^2 \right]}_{t_1^{\text{SI,MRT}}} + \underbrace{\mathbb{E} \left[\left| a_k \hat{\mathbf{h}}_k^T \mathbf{C}' \hat{\mathbf{h}}_k^* s_k \right|^2 \right]}_{t_2^{\text{SI,MRT}}} + \underbrace{\mathbb{E} \left[\left| a_k \boldsymbol{\varepsilon}_k^T \mathbf{C} \hat{\mathbf{h}}_k^* s_k \right|^2 \right]}_{t_3^{\text{SI,MRT}}} \right. \\
&\quad \left. - \underbrace{\mathbb{E} \left[\left| \frac{N \tau_u \rho_u}{\tau_u \rho_u + 1} s_k \right|^2 \right]}_{t_4^{\text{SI,MRT}}} \right). \tag{51}
\end{aligned}$$

Next we derive analytical expressions for the terms $t_1^{\text{SI,MRT}}$, $t_2^{\text{SI,MRT}}$, $t_3^{\text{SI,MRT}}$, and $t_4^{\text{SI,MRT}}$. Starting with $t_1^{\text{SI,MRT}}$, we get

$$\begin{aligned}
t_1^{\text{SI,MRT}} &= \mathbb{E} \left[\left| a_k \hat{\mathbf{h}}_k^T \hat{\mathbf{h}}_k^* s_k \right|^2 \right] = \mathbb{E} [|a_k|^2] \mathbb{E} \left[\left(\sum_{l=1}^N \hat{h}_{kl} \hat{h}_{kl}^* \right) \left(\sum_{q=1}^N \hat{h}_{kq} \hat{h}_{kq}^* \right)^* \right] \mathbb{E} [|s_k|^2] \\
&= N (N + 1) (1 + \sigma_A^2) \left(\frac{\tau_u \rho_u}{\tau_u \rho_u + 1} \right)^2.
\end{aligned} \tag{52}$$

Then, we can express $t_2^{\text{SI,MRT}}$ as

$$\begin{aligned}
t_2^{\text{SI,MRT}} &= \mathbb{E} \left[\left| a_k \hat{\mathbf{h}}_k^T \mathbf{C}' \hat{\mathbf{h}}_k^* s_k \right|^2 \right] = (1 + \sigma_A^2) \sum_{l=1}^N \sum_{q=1}^N \mathbb{E} \left[\hat{h}_{kl} \hat{h}_{kl}^* \hat{h}_{kq} \hat{h}_{kq}^* \right] \mathbb{E} [c'_{lq} c'_{lq}^*] \\
&= N (1 + \sigma_A^2) \left(\frac{\tau_u \rho_u}{\tau_u \rho_u + 1} \right)^2 (2\sigma_{C_d}^2 + (N - 1) \sigma_{C_{od}}^2).
\end{aligned} \tag{53}$$

In obtaining the right-hand side of the equation on the first line, we used Property 1.

Following that, $t_3^{\text{SI,MRT}}$ can be expressed as

$$\begin{aligned} t_3^{\text{SI,MRT}} &= \mathbb{E} \left[\left| a_k \boldsymbol{\varepsilon}_k^T \mathbf{C} \hat{\mathbf{h}}_k^* s_k \right|^2 \right] = (1 + \sigma_A^2) \sum_{l=1}^N \sum_{q=1}^N \mathbb{E}[\epsilon_{kl} \epsilon_{kl}^*] \mathbb{E}[c_{lq} c_{lq}^*] \mathbb{E}[\hat{h}_{kq} \hat{h}_{kq}^*] \\ &= \frac{N(1 + \sigma_A^2) \tau_u \rho_u}{(\tau_u \rho_u + 1)^2} (1 + \sigma_{C_d}^2 + (N-1) \sigma_{C_{od}}^2). \end{aligned} \quad (54)$$

In obtaining the right-hand side of the equation on the first line, we used Property 2 and Property 4.

Lastly, $t_4^{\text{SI,MRT}}$ is given as

$$t_4^{\text{SI,MRT}} = \mathbb{E} \left[\left| \frac{N \tau_u \rho_u}{\tau_u \rho_u + 1} s_k \right|^2 \right] = N^2 \left(\frac{\tau_u \rho_u}{\tau_u \rho_u + 1} \right)^2. \quad (55)$$

The power of self-interference under MRT precoding can be then analytically expressed by plugging (52)–(55) into (51), which yields

$$\begin{aligned} \text{Var} \left(z_k^{\text{SI,MRT}} \right) &= \rho_d \frac{(N+1)(1 + \sigma_A^2) \tau_u \rho_u}{K(\tau_u \rho_u + 1)} + \rho_d \frac{(1 + \sigma_A^2) \tau_u \rho_u}{K(\tau_u \rho_u + 1)} (2\sigma_{C_d}^2 + (N-1) \sigma_{C_{od}}^2) \\ &\quad + \rho_d \frac{1 + \sigma_A^2}{K(\tau_u \rho_u + 1)} (1 + \sigma_{C_d}^2 + (N-1) \sigma_{C_{od}}^2) - \rho_d \frac{N \tau_u \rho_u}{K(\tau_u \rho_u + 1)}. \end{aligned} \quad (56)$$

Then, based on (16), the power of IUI under MRT precoding scheme can be written as

$$\begin{aligned} \text{Var} \left(z_k^{\text{IUI,MRT}} \right) &= \mathbb{E} \left[\left| \sqrt{\rho_d} \sum_{i=1, i \neq k}^K \beta^{\text{MRT}} a_k \left(\hat{\mathbf{h}}_k^T + \boldsymbol{\varepsilon}_k^T \right) \mathbf{C} \hat{\mathbf{h}}_i^* s_i \right|^2 \right] \\ &= (K-1) \rho_d (\beta^{\text{MRT}})^2 \left(\underbrace{\mathbb{E} \left[\left| a_k \hat{\mathbf{h}}_k^T \mathbf{C} \hat{\mathbf{h}}_i^* s_i \right|^2 \right]_{i \neq k}}_{t_1^{\text{IUI,MRT}}} + \underbrace{\mathbb{E} \left[\left| a_k \boldsymbol{\varepsilon}_k^T \mathbf{C} \hat{\mathbf{h}}_i^* s_i \right|^2 \right]_{i \neq k}}_{t_2^{\text{IUI,MRT}}} \right). \end{aligned} \quad (57)$$

Next, we will derive analytical expressions for the terms $t_1^{\text{IUI,MRT}}$ and $t_2^{\text{IUI,MRT}}$. Starting with $t_1^{\text{IUI,MRT}}$, we get

$$\begin{aligned} t_1^{\text{IUI,MRT}} &= \mathbb{E} \left[\left| a_k \hat{\mathbf{h}}_k^T \mathbf{C} \hat{\mathbf{h}}_i^* s_i \right|^2 \right]_{i \neq k} = (1 + \sigma_A^2) \sum_{l=1}^N \sum_{q=1}^N \mathbb{E}[\hat{h}_{kl} \hat{h}_{kl}^*] \mathbb{E}[c_{lq} c_{lq}^*] \mathbb{E}[\hat{h}_{iq} \hat{h}_{iq}^*]_{i \neq k} \\ &= N(1 + \sigma_A^2) \left(\frac{\tau_u \rho_u}{\tau_u \rho_u + 1} \right)^2 (1 + \sigma_{C_d}^2 + (N-1) \sigma_{C_{od}}^2). \end{aligned} \quad (58)$$

In obtaining the right-hand side of the equation on the first line, we used Property 4.

Following that, $t_2^{\text{IUI,MRT}}$ can be expressed as

$$\begin{aligned} t_2^{\text{IUI,MRT}} &= \mathbb{E} \left[\left| a_k \mathbf{\epsilon}_k^T \mathbf{C} \hat{\mathbf{h}}_i^* s_i \right|^2 \right] = (1 + \sigma_A^2) \sum_{l=1}^N \sum_{q=1}^N \mathbb{E}[\epsilon_{kl} \epsilon_{kl}^*] \mathbb{E}[c_{lq} c_{lq}^*] \mathbb{E}[\hat{h}_{iq} \hat{h}_{iq}^*] \\ &= \frac{N (1 + \sigma_A^2) \tau_u \rho_u}{(\tau_u \rho_u + 1)^2} (1 + \sigma_{C_d}^2 + (N - 1) \sigma_{C_{od}}^2). \end{aligned} \quad (59)$$

In obtaining the right-hand side of the equation on the first line, we used Property 4.

The power of the IUI under MRT precoding scheme can be analytically expressed by plugging (58) and (59) into (57) which yields

$$\text{Var} \left(z_k^{\text{IUI,MRT}} \right) = \rho_d \frac{(K - 1) (1 + \sigma_A^2)}{K} (1 + \sigma_{C_d}^2 + (N - 1) \sigma_{C_{od}}^2). \quad (60)$$

Finally, the total interference power is obtained by summing $\text{Var} \left(z_k^{\text{SI,MRT}} \right)$ and $\text{Var} \left(z_k^{\text{IUI,MRT}} \right)$ from (56) and (60), respectively. Then, it is straightforward to re-arrange the terms and express the total interference power as $I_{\text{RC}}^{\text{MRT}} + I_{\text{NRC}}^{\text{MRT}}$ after which we reach the SINR expression presented in (27).

REFERENCES

- [1] J. G. Andrews, S. Buzzi, W. Choi, S. V. Hanly, A. Lozano, A. C. K. Soong, and J. C. Zhang, "What will 5G be?" *IEEE Journal on Selected Areas in Communications*, vol. 32, no. 6, pp. 1065–1082, June 2014.
- [2] F. Boccardi, R. Heath, A. Lozano, T. L. Marzetta, and P. Popovski, "Five disruptive technology directions for 5G," *IEEE Communications Magazine*, vol. 52, no. 2, pp. 74–80, February 2014.
- [3] J. Hoydis, S. ten Brink, and M. Debbah, "Massive MIMO in the UL/DL of cellular networks: how many antennas do we need?" *IEEE Journal on Selected Areas in Communications*, vol. 31, no. 2, pp. 160–171, February 2013.
- [4] L. Lu, G. Y. Li, A. L. Swindlehurst, A. Ashikhmin, and R. Zhang, "An overview of massive MIMO: benefits and challenges," *IEEE Journal of Selected Topics in Signal Processing*, vol. 8, no. 5, pp. 742–758, Oct 2014.
- [5] T. L. Marzetta, "Noncooperative cellular wireless with unlimited numbers of base station antennas," *IEEE Transactions on Wireless Communications*, vol. 9, no. 11, pp. 3590–3600, November 2010.
- [6] H. Q. Ngo, E. G. Larsson, and T. L. Marzetta, "Energy and spectral efficiency of very large multiuser MIMO systems," *IEEE Transactions on Communications*, vol. 61, no. 4, pp. 1436–1449, April 2013.
- [7] H. Yang and T. L. Marzetta, "Performance of conjugate and zero-forcing beamforming in large-scale antenna systems," *IEEE Journal on Selected Areas in Communications*, vol. 31, no. 2, pp. 172–179, February 2013.
- [8] X. Gao, O. Edfors, F. Rusek, and F. Tufvesson, "Linear pre-coding performance in measured very-large MIMO channels," in *Vehicular Technology Conference (VTC Fall), 2011 IEEE*, Sept 2011, pp. 1–5.
- [9] M. Kobayashi, N. Jindal, and G. Caire, "Training and feedback optimization for multiuser MIMO downlink," *IEEE Transactions on Communications*, vol. 59, no. 8, pp. 2228–2240, August 2011.
- [10] E. G. Larsson, O. Edfors, F. Tufvesson, and T. L. Marzetta, "Massive MIMO for next generation wireless systems," *IEEE Communications Magazine*, vol. 52, no. 2, pp. 186–195, February 2014.
- [11] J. Haartsen, "Impact of non-reciprocal channel conditions in broadband TDD systems," in *IEEE 19th International Symposium on Personal, Indoor and Mobile Radio Communications (PIMRC)*, Sept 2008, pp. 1–5.
- [12] A. Bourdoux, B. Come, and N. Khaled, "Non-reciprocal transceivers in OFDM/SDMA systems: impact and mitigation," in *Radio and Wireless Conference, 2003. RAWCON '03. Proceedings*, Aug 2003, pp. 183–186.
- [13] J. Liu, A. Bourdoux, J. Craninckx, P. Wambacq, B. Come, S. Donnay, and A. Barel, "OFDM-MIMO WLAN AP front-end gain and phase mismatch calibration," in *Radio and Wireless Conference, 2004 IEEE*, Sept 2004, pp. 151–154.

- [14] B. Kouassi, I. Ghauri, and L. Deneire, "Estimation of time-domain calibration parameters to restore MIMO-TDD channel reciprocity," in *7th International ICST Conference on Cognitive Radio Oriented Wireless Networks and Communications (CROWNCOM)*, June 2012, pp. 254–258.
- [15] M. Petermann, M. Stefer, F. Ludwig, D. Wubben, M. Schneider, S. Paul, and K.-D. Kammeyer, "Multi-user pre-processing in multi-antenna OFDM TDD systems with non-reciprocal transceivers," *IEEE Transactions on Communications*, vol. 61, no. 9, pp. 3781–3793, September 2013.
- [16] Y. Zou, O. Raeesi, R. Wichman, A. Tolli, and M. Valkama, "Analysis of channel non-reciprocity due to transceiver and antenna coupling mismatches in TDD precoded multi-user MIMO-OFDM downlink," in *IEEE 80th Vehicular Technology Conference (VTC Fall)*, Sept 2014, pp. 1–7.
- [17] S. Durrani and M. E. Bialkowski, "Effect of mutual coupling on the interference rejection capabilities of linear and circular arrays in CDMA systems," *IEEE Transactions on Antennas and Propagation*, vol. 52, no. 4, pp. 1130–1134, April 2004.
- [18] O. Raeesi, Y. Zou, A. Tolli, and M. Valkama, "Closed-form analysis of channel non-reciprocity due to transceiver and antenna coupling mismatches in multi-user massive MIMO network," in *IEEE Global Communications Conference Workshops (GLOBECOM)*, Dec 2014, pp. 333–339.
- [19] H. Wei, D. Wang, and X. You, "Reciprocity of mutual coupling for TDD massive MIMO systems," in *Wireless Communications Signal Processing (WCSP), 2015 International Conference on*, Oct 2015, pp. 1–5.
- [20] F. Athley, G. Durisi, and U. Gustavsson, "Analysis of massive MIMO with hardware impairments and different channel models," in *2015 9th European Conference on Antennas and Propagation (EuCAP)*, May 2015, pp. 1–5.
- [21] H. Wei, D. Wang, J. Wang, and X. You, "Impact of RF mismatches on the performance of massive MIMO systems with ZF precoding," *Science China Information Sciences*, vol. 59, no. 2, pp. 1–14, 2016. [Online]. Available: <http://dx.doi.org/10.1007/s11432-015-5509-1>.
- [22] W. Zhang, H. Ren, C. Pan, M. Chen, R. de Lamare, B. Du, and J. Dai, "Large-scale antenna systems with UL/DL hardware mismatch: achievable rates analysis and calibration," *IEEE Transactions on Communications*, vol. 63, no. 4, pp. 1216–1229, April 2015.
- [23] J. Jose, A. Ashikhmin, P. Whiting, and S. Vishwanath, "Channel estimation and linear precoding in multiuser multiple-antenna TDD systems," *IEEE Transactions on Vehicular Technology*, vol. 60, no. 5, pp. 2102–2116, Jun 2011.
- [24] J. Jose, A. Ashikhmin, T. L. Marzetta, and S. Vishwanath, "Pilot contamination and precoding in multi-cell TDD systems," *IEEE Transactions on Wireless Communications*, vol. 10, no. 8, pp. 2640–2651, August 2011.
- [25] H. Q. Ngo, E. G. Larsson, and T. L. Marzetta, "Massive MU-MIMO downlink TDD systems with linear precoding and downlink pilots," in *51st Annual Allerton Conference on Communication, Control, and Computing (Allerton)*, Oct 2013, pp. 293–298.
- [26] —, "The multicell multiuser MIMO uplink with very large antenna arrays and a finite-dimensional channel," *IEEE Transactions on Communications*, vol. 61, no. 6, pp. 2350–2361, June 2013.
- [27] Evolved Universal Terrestrial Radio Access (E-UTRA); Physical channels and modulation, The 3rd Generation Partnership Project (3GPP) Tech. Spec., V13.1.0, Release 13, TS 36.211, March 2016.

TABLE I
MOST IMPORTANT VARIABLES USED THROUGHOUT THE PAPER

Variable	Dimensions	Definition
\mathbf{A}	$K \times K$	Channel non-reciprocity matrix at UE side
\mathbf{A}'	$K \times K$	Non-ideal part of NRC matrix at UE side
\mathbf{B}	$N \times N$	Frequency-response matrix of the BS
\mathbf{C}	$N \times N$	Channel non-reciprocity matrix in the BS
\mathbf{C}'	$N \times N$	Non-ideal part of channel non-reciprocity matrix in the BS
\mathbf{F}	$K \times K$	Frequency-response matrix of the UEs
\mathbf{G}	$N \times K$	Effective UL channel matrix
$\hat{\mathbf{G}}$	$N \times K$	Estimated UL channel matrix
\mathbf{H}	$K \times N$	Effective DL channel matrix
$\hat{\mathbf{H}}$	$K \times N$	Estimated DL channel matrix
I_{NRC}	scalar	Contribution of interference and noise power due to NRC
I_{RC}	scalar	Contribution of interference and noise power under ideal reciprocal channel
K	scalar	Number of single-antenna UEs
\mathbf{M}	$N \times N$	Antenna mutual coupling matrix of the BS
\mathbf{n}	$K \times 1$	Additive receiver noise at the UE side
N	scalar	Number of antennas in the BS
\mathbf{N}^p	$N \times \tau_u$	Additive receiver noise at the BS during UL pilot transmission
\mathbf{P}	$N \times K$	(Reciprocal) Physical channel matrix
\mathbf{Q}	$N \times K$	Processed receiver noise at the BS during UL pilot transmission
\mathbf{r}	$K \times 1$	Received DL data vector corresponding to all the UEs
R	scalar	Capacity lower bound of the system
\mathbf{s}	$K \times 1$	DL user data vector
T	scalar	Number of symbols in each channel coherence interval
\mathbf{U}	$N \times K$	Linear precoder matrix
\mathbf{x}	$N \times 1$	Precoded DL transmit signal vector at the BS
\mathbf{X}^p	$K \times \tau_u$	Matrix of UL pilots from all the UEs
\mathbf{Y}	$N \times K$	Processed received signal at the BS during UL pilot transmission
\mathbf{Y}^p	$N \times \tau_u$	Received signal at the BS during UL pilot transmission
z_k^{IUI}	scalar	Inter-user interference at the k -th UE
z_k^{SI}	scalar	Self interference at the k -th UE
α	scalar	Relative SINR degradation
β	scalar	Transmit power normalization factor
\mathcal{E}	$K \times N$	UL channel estimation error
η_s	scalar	Spectral efficiency
ρ_d	scalar	Transmit SNR of the DL channel
ρ_u	scalar	Transmit SNR of the UL channel
$\sigma_{\mathbf{A}}^2$	scalar	Power of channel non-reciprocity at the UE side
$\sigma_{\mathbf{C}_d}^2$	scalar	Power of diagonal elements of BS NRC matrix
$\sigma_{\mathbf{C}_{od}}^2$	scalar	Power of off-diagonal elements of BS NRC matrix
τ_u	scalar	Number of orthogonal pilot symbols sent by each UE in each channel coherence interval